Research Square

Preprints are preliminary reports that have not undergone peer review.
They should not be considered conclusive, used to inform clinical practice,
or referenced by the media as validated information.

The adsorption performance, thermodynamic and kinetic model of high crystallinity Na-p zeolites prepared from oil shale ash for the waste water treatment

Xuejian Zhang
Jilin Jianzhu University
Rui Wang
Jilin Jianzhu University
Fanping Meng
China North standardization Center
Yongtao Li
lyt45628740163.com

Jilin Jianzhu University
Jie Chen
Jilin Jianzhu University
Yusheng Gao
Ji Lin Jian Zhu University
Jinyi Zhang
Jilin Jianzhu University
Weidong Ai
Jilin Jianzhu University
Kuishan Wang
Jilin Jianzhu University
Chenyang Zhang
Jilin Jianzhu University
C. K. Mahadevan
CSIR Emeritus Scientist, Bharathidasan University

Research Article

Keywords: Zeolite material, OSA and CFA, Absorption, Methylene blue, Thermodynamic and kinetic

Posted Date: January 24th, 2024

DOI: https://doi.org/10.21203/rs.3.rs-3881683/v1

License: This work is licensed under a Creative Commons Attribution 4.0 International License.
Read Full License

Additional Declarations: No competing interests reported.

The adsorption performance, thermodynamic and kinetic model of high crystallinity Na-p zeolites prepared from oil shale ash for the waste water treatment

Xuejian Zhang[a], Rui Wang[a], Fanping Meng[b], Yongtao Li[a,c]*, Jie Chen[a], Yusheng Gao[c], Jinyi Zhang[a], Weidong Ai[a], Kuishan Wang[a], Chenyang Zhang[a], C.K.Mahadevan[d]**

([a]School of Materials Science and Engineering, Jilin Jianzhu University, Changchun, 130018, China

[b]China North standardization Center, Beijing 100089, China

[c]School of Emergency Science and Engineering, Ji Lin Jian Zhu University, Changchun, 130018, China

[d]CSIR Emeritus Scientist, Department of Physics, Bharathidasan University, Tiruchirappalli, Tamil Nadu,620024, India)

**Corresponding author* ***Corresponding author*

lyt4562874@163.com (Y. Li), zhangjinyi_jlju@163.com.(J. Zhang)

Abstracts: The Na-p zeolite using oil shale ash (OSA) as raw material was synthesized by hydrothermal synthesis method. The effects of alkali concentration, acid concentration, crystallization temperature, and crystallization time on the formation of Na-p zeolite were studied. The optimal synthesis conditions for converting oil shale ash into Na-p zeolite are: acid leaching concentration is 10%, NaOH dosage is 7 g, crystallization temperature is 130℃ and crystallization time is 12 h. It is found that adding some coal fly ash to oil shale ash can improve the adsorption performance of zeolite materials. The specific surface and the crystallinity of zeolite prepared from OSA and coal fly ash (CFA) are greater than that of pure OSA. The absorbion experiment results indicate that the zeolite synthesized by adding coal fly ash to the oil shale ash own richer pore structure and higher adsorption efficiency for methylene blue (99.2%). The thermodynamic and kinetic processes of methylene blue adsorption by pure oil shale ash, zeolites synthesized from oil shale ash, and zeolites synthesized from oil shale ash with coal fly ash have been systematically studied. These results reveal that the zeolite synthesized in the present study with high absorption can be used as a promising material for the wast water treatment.

Keywords: Zeolite material; OSA and CFA; Absorption; Methylene blue;

Thermodynamic and kinetic

1. Introduction

Methylene blue (MB) is extensively used in chemical indicators, pharmaceutical drugs, and biological stains [1-3]. MB is an organic dye soluble in water, and its aqueous solution proves alkaline and toxic [4]. The inhalation of MB through the nose can lead to respiratory disease[5]. Accidental contact with human or animal eyes can cause burns and lasting damage. Ingestion through the mouth may cause rapid heart rate, nausea, and vomiting in humans [6-8]. Therefore, scientists have focused much attention on remediating water bodies contaminated with MB. At present, activated carbon is the most effective adsorbent [9]. However, it is limited due to the high cost and complicate manufacturing process [10]. Thus, the development of a low-cost and easily prepared absorption material has become urgent [11].

Solid waste materials such as coal fly ash (CFA) and oil shale ash (OSA) have been widely produced in the past years. Just in 2023, the production of CFA and OSA are 8.65×10^8 and 7.03×10^5 t respectively. At present, the majority of solid waste is arbitrarily stacked in the open air, which has seriously acidified the land damaged the environment, polluted the air, and jeopardized human health [12-14]. Therefore, many researchers have studied the comprehensive utilization of OSA and CFA. Liu et al. successfully produced mesoporous silica microspheres using waste coal gasification fine slag as a silicon source. Methylene blue adsorption test was conducted on the prepared mesoporous microspheres, and the maximum adsorption capacity was 140.57 mg/g [15]. Bai et al. used OSA as raw material to synthesize Na-x zeolite by alkaline melting method [16]. Adnan et al. successfully converted OSA to Na-p1 type zeolite by alkaline thermal activation with sodium hydroxide and studied its adsorption model for cadmium and lead ions [17]. Li et al. successfully synthesized activated carbon/zeolite composites as adsorbents for the removal of heavy metal ions and macromolecules of organic matter by using gangue as raw material through carbon dioxide activation and hydrothermal synthesis methods, which showed high adsorption efficiency for Cu^{2+} (92.8%) and Rh-B (94.2%) [18]. Bao et al. synthesized zeolite A from OSA for the adsorption of copper ion solution, and found that the maximum adsorption capacity was 156.7 mg/g [19]. Tomasz et al. conducted a hydrothermal synthesis of CFA and studied the effect of the initial dissolution stage on the synthesis of zeolite to more clearly describe the relationship between the synthesis conditions and the resulting products [20]. Tunde et al. successfully synthesized zeolite A using CFA as raw material by ultrasonic chemical treatment [21]. However, the study on the preparation of adsorbent materials from mixed types of solid wastes has not been reported. Thus, the preparation of adsorbent materials from acid-treated OSA and CFA as raw materials and the adsorption efficiency of macromolecular dyestuffs were investigated.

In this paper, the Na-p zeolite has been successfully synthesized by the pure OSA and introduced CFA into OSA. The absorption kinetics and adsorption kinetics and adsorption thermodynamics of MB on OSA and Na-p zeolite prepared with different raw materials. The results obtained in this paper indicated that the Na-zeolite prepared can be

used for waste water and organic dye treatment.

2. Experimental section

2.1. Materials

The CFA and OSA were obtained from Jilin Province. Methylene blue (MB, 98%) and sodium hydroxide (NaOH, 96%) were produced by Tianjin Guangfu Institute of Fine Chemicals and Shanghai Wokai Biotechnology Co., respectively.

2.2. preparation of Na-p zeolite

OSA and CFA were ground into powder separately at 360 r/min by using the ball mill and subsequently filtered through a 200-mesh screen (particle sizes<0.075 mm). The OSA powder obtained was soaked in a 10% hydrochloric acid solution for 3 h to eliminate excess impurities. The remaining material was filtered and washed until the filtrate pH was 7 and then dried to obtain an acid-leaching raw material of OSA. The treated oil shale ash with a weight of 3 g was mixed with 7 g of NaOH in 50 ml of deionized water. The final mixture was agitated well and placed in a 50 ml stainless steel reactor with a PTFE-lined for a hydrothermal reaction at 120°C for 12 h. After the reaction was completed, the mixture was separated by a high-speed centrifuge. The remaining solids were repeatedly cleaned with deionized water until neutral. It was subsequently dried in an oven at 60°C for 10 h. The synthesized zeolite from OSA was noted as Na-p(o). The second sample called Na-p(f) was ground with 2 g of OFA and 3 g of OSA.The preparation method of Na-p(f) zeolite is same as that of Na-p(o) zeolite.

2.3. characterization

The scanning electron microscope (SEM) provided by Wuxi Novolit Automation Equipment Co., Ltd. in China with an accelerating voltage of 25 kV and a vacuum of 20 Pa an the Transmission electron microscope (TEM) with model JEOL JEM-F 200 of Japan with an accelerating voltage of 200 kV were used to study the morphology. The ray diffractometer (XRD) from SmartLab was used to study the phase composition of the zeolite. The zeolite was measured by X-ray diffractometer with a voltage of 40 kV and a current of 40 mA. The composition of the material and the structure of its internal atoms or molecules. Fourier transform infrared spectroscopy with a scanning range of 500-4000 cm^{-1}.(FTIR, Nicolet iS5, Thermo Fisher Scientific, USA) was used to identify the presence or changes of functional groups and chemical bonds in the sample. The automated specific surface area and porosity analyzer (TriStar, V-Sorb X800, Beijing Guoyi Precision Measurement Technology Co., Ltd, China) was employed to determine specific surface area and pore structure.

2.4. Adsorption experiments

The concentration of the solution was measured using a UV-visible spectrophotometer (UV 1700, Beijing Pu Analytical General Instrument Co., Ltd., China) with a wavelength spectrum of 600-800. To carry out the MB adsorption experiments, 0.05 g of zeolite was added to a 50 ml liquid containing 35 mg/l of MB, and the mixture was stirred for 180 min. Then, 10 ml of the supernatant solution of MB was obtained and centrifuged at 8000 r/min for 3 minutes. The concentration of the obtained solution was

determined using a UV-spectrophotometer. The values of *R* and *Qe* were determined using the following equations [22, 23].

$$R = (C_o - C_e)/C_o \times 100\% \quad (1)$$

$$Q_e = (C_o - C_e) \times V/m \quad (2)$$

3. Results and discuss

3.1. Phase structure of Na-p(o) and Na-p(f) zeolite

Fig. 1 displays the XRD patterns of the synthesized zeolites under different synthesis conditions. It can be seen from Fig. 1 (a) that the diffraction peaks of the sodium aluminosilicate phase structure in the zeolite increase with the increment of the NaOH dosage, suggesting that an increase in NaOH dosage can promote the solubility of silicon and aluminum in OSA during the process of alkali melting.

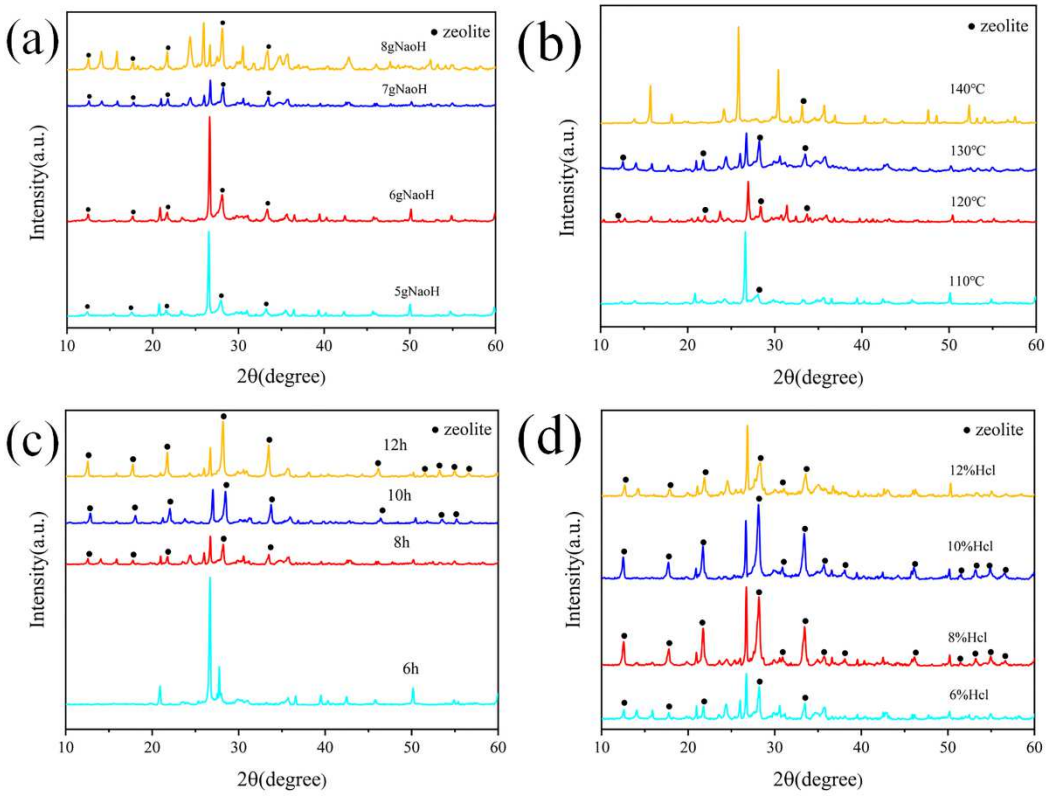


Fig. 1. XRD patterns of zeolite under different preparation conditions (a) alkali concentrations; (b) crystallization temperatures; (c) crystallization times; and (d) acid leaching concentrations.

Fig. 1 (b) depicts the effect of crystallization temperatures. It is worth noting that the Na-p zeolite is formed when temperatures are below 130℃, while the Na-p zeolite disappears after the temperatures increase to 140℃. Fig. 1 (c) shows the XRD patterns of the hydrothermal products at different crystallization times, the diffraction peaks intensity of the zeolite increase as the reaction time increases, indicating that extending the

crystallization time can improve the crystallinity of zeolite, which is in agreement with the previous work reported by Liu et al. [24]. Fig. 1 (d) displays the XRD pattern of synthesized zeolites with different acid-leaching concentrations. When the concentration of hydrochloric acid was within 10%, the intensity of the zeolite diffraction peak increases as the concentration of hydrochloric acid increases. The diffraction peak intensity of Na-p zeolite decreases when the concentration of hydrochloric acid increases to 12%. Based on the results, we can conclude that the optimal conditions for the synthesis of Na-p(o) zeolite are: the amount of NaOH is 7 g, the hydrothermal temperature is 130℃, the hydrothermal time is 12 h, and the HCl concentration is 10%.

Fig. 2 displays XRD patterns of Na-p(o) and Na-p(f) prepared with the method as that of the Na-p(o) zeolite. It is evident that the several peak lie at 12.5°, 17.7°, 28.2°, 33.5°, 46.2°, 51.7°, 53.4° and 55.1°, which are identical to those of JCPDS 25-0778, confirming that two samples are molecular sieves of Na-p type. However, there are notable differences in both the peaks of crystalline silica and the crystallinity of the two samples, as observed from the XRD patterns. For the peak at 26.6° of crystalline silica, the peak intensity of Na-p(f) is less than that of Na-p(o), whereas for the other peaks, the intensity of Na-p(f) is greater than that of Na-p(o). To further quantify the difference in crystallinity, the equation (3) was used to estimate crystallinity [25]:

$$C_o = A_c/(A_a + kA_c) \times 100\% \qquad (3)$$

Here, A_c is the total of the crystalline peak areas, A_a is the amorphous phase area, and k is the relative scattering coefficient, which is initially set to 1. The crystallinity of Na-p(o) and Na-p(f) was 64.07% and 86.32%, respectively. Thus, the crystallinity of the Na-p(f) zeolite is higher than the Na-p(o) zeolite.

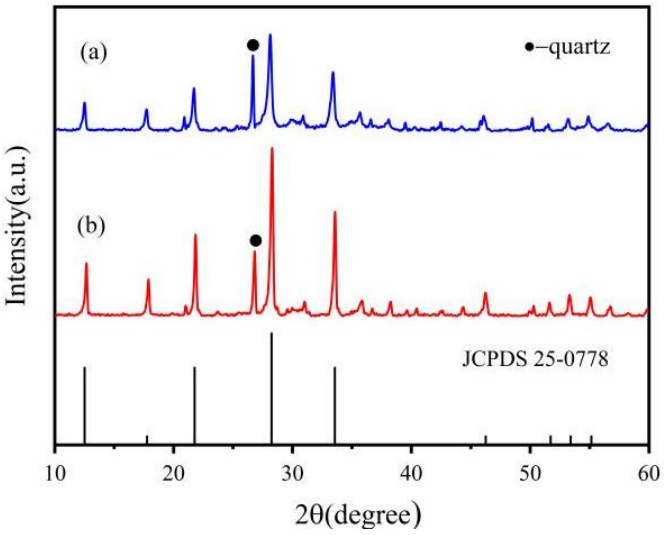


Fig. 2. XRD patterns of (a) Na-p(o) ; (b)Na-p(f)

The morphology of OSA, Na-p(o), and Na-p(f) is analyzed using SEM and TEM. Which is shown in Fig. 3, the SEM shows that the OSA powder is composed of irregular particles, spherical particles, and irregular hollow particles. The edges of the particles are serrated and the particle size distribution is uneven. Aluminosilicate exists in the form of

irregular particles and spherical particles, and impurity elements such as Fe, Mg, Ca, and Na are also presented [26]. Fig. 3 (a) and (b) show the SEM and low magnification TEM images of Na-p(o), respectively. From Fig. 3 (a), it can be observed that the sample transforms from an irregular shape to a surface spherical particle, while Fig. 3 (b) shows that the surface of the spherical particle is columnar [27]. The SEM and low magnification TEM images of Na-p(f) are displayed in Fig. 3 (d) and (e). It is shown that the pseudo-spherical particles are transformed into clear crystal edges of "diamond" shaped particles. The zeolite of "diamond" shaped particles have better crystallinity than pseudo-spherical particles, which is in agreement with the earlier results reported by Huo et al [28]. The selected region electron diffractions presented in Fig. 3 (c) and Fig. 3 (f), respectively, confirming that the crystallinity of Na-p(f) zeolite is higher than that of Na-p(o), which is consistent with the inferred results of SEM. The high-resolution TEM image of Na-p(f) in Fig. 3 (h) shows that the distance between adjacent planes is 0.35 nm, which is in agreement with the crystal plane of zeolite (100).

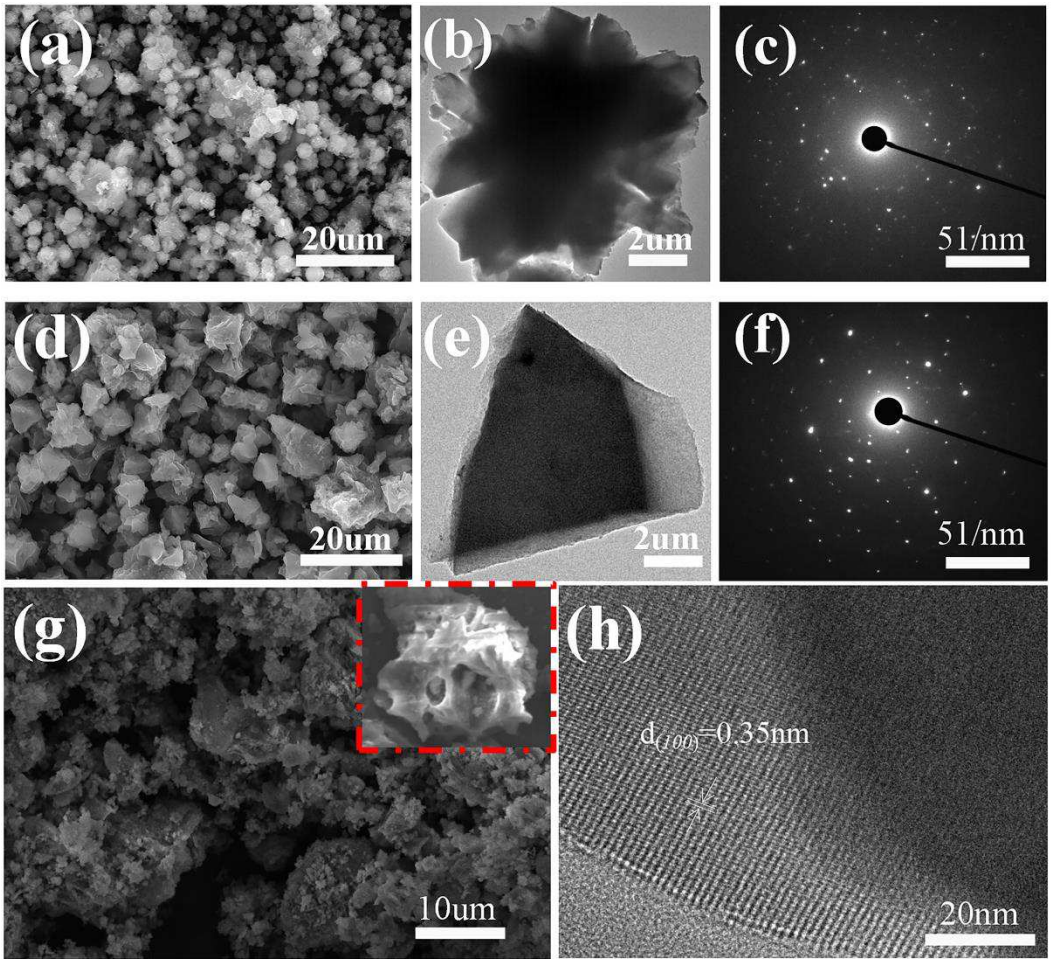


Fig. 3. (a) SEM images of Na-p(o) ; (b) low magnification of Na-p(o); (c) TEM images ofand selected area electron diffractions of Na-p(o) ; (d) SEM images of Na-p(f) ; (e) low magnification of Na-p(f); (f) TEM images ofand selected area electron diffractions of Na-p(f) ; (g) SEM image of OSA; (h) High-resolution TEM image of Na-p(f)

The Fourier Transform Infrared (FT-IR) spectrometer is based on the principle that molecules can selectively absorb infrared light at particular wavelengths, leading to changes in vibration and rotational energy levels [29]. FT-IR spectroscopy is used to examine the chemical bonds and functional groups of products as a means of obtaining information about the molecular structure of the material [30]. Fig. 4 illustrates the infrared spectra of Na-P(o), and Na-p(f). The band at 3445 cm^{-1} belongs to the stretching vibrations of the OH group [31]. The strong absorption peak at 1008 cm^{-1} corresponds to asymmetric stretching vibrations of Si-O or Al-O, and the peak in the 400-500 cm^{-1} is related to bending vibrations of Si-O or Al-O [32, 33]. The peak center at 1008cm^{-1} and 400-500cm^{-1} prove the transformation of OSA and CFA into Na-p zeolite. The bands in the 600-760 cm^{-1} can be attributed to the symmetric tensile vibration absorption of the internal tetrahedra [34]. As shown in Fig. 4, the vibrational amplitude of the infrared spectrum of Na-p(f) zeolite is larger than that of Na-p(o) zeolite, indicating that the zeolite content of Na-p(f) exceeds that of Na-p(o), which aligns with the results of SEM and XRD.

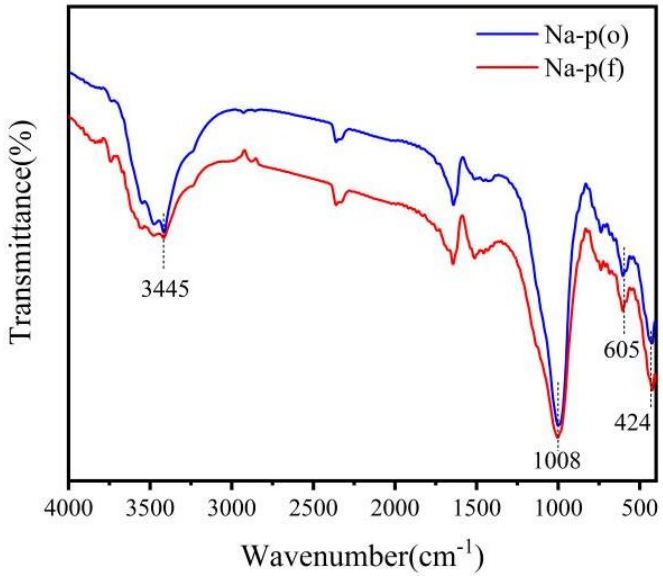


Fig. 4. Infrared spectra of Na-p(o), Na-p(f) zeolite.

Static volumetric gas adsorption is used to examine the specific surface area of zeolites. Fig. 5 shows the adsorption-desorption isotherms of Na-p(f) and Na-p(o). The Na-p(o) samples are classified as having type III isotherms accompanied by H2 hysteresis loops. Weak adsorption is observed when $P/P_0 < 0.05$, while the hysteresis loop at $P/P_0 > 0.5$ indicates the existence of mesoporous. This effect is attributed to pore connectivity and the presence of narrow orifices in the pore channels [35]. For the Na-p(f) sample, isotherms were assigned to type III with H3 hysteresis loops. The hysteresis loops show a slight increase in the adsorption comparing with to the Na-p(o) sample at $P/P_0 <0.05$ in the low-pressure region, and a significant increase at $P/P_0 >0.6$ in the high-pressure region, suggesting that the incorporation of CFA into OSA leads to the formation of a higher number of mesoporous and macropores [18]. The specific surface area of the Na-p(o)

zeolite and Na-p(f) zeolite is 20.6 m^2/g and 59.6 m^2/g, respectively. These results indicate that the presence of CFA increases the diversity of the pore structure and significantly increases the specific surface area of the zeolite.

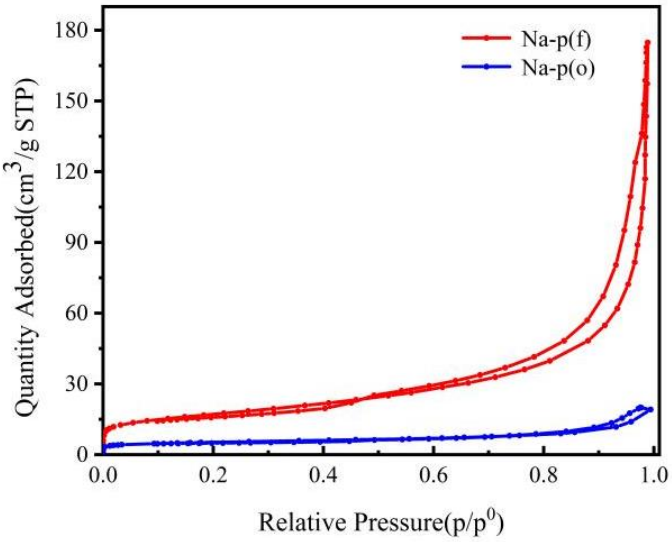


Fig. 5. Adsorption-desorption isotherms of Na-p(f) and Na-p(o).

3.2. MB adsorption performance of Na-p zeolite

3.2.1. The adsorption efficiency of Na-p zeolite

In order to evaluate the adsorption performance of zeolites synthesized from different raw materials, the samples of OSA, Na-p(f), and Na-p(o) are put into MB solutions representing organic pollutants. Fig. 6 (a-c) shows the MB aqueous solution onto different samples as a function of time. The MB concentration dropped significantly at 70 min. It can be concluded that the absorbance of three samples decreased with the increment of the reaction time, which is related to the presence of vacant adsorption sites on the surface of the samples and a high concentration of MB in the solution [36]. When OSA, Na-p(o), and Na-p(f) samples reached adsorption equilibrium for MB solution, the adsorption efficiencies were 27.6%, 83.4%, and 99.2%, respectively, which are displayed in Fig. 6(d). Moreover, int can be seen that the OSA has low pollutant adsorption capability. The limited adsorption capabilities of Na-p(o) (zeolite from OSA) for macromolecular organic pollutants are due to its narrow pore size, which restricts the adsorption of macromolecular dyes onto the zeolite surface. When introducing CFA into OSA to prepare Na-p(f), the adsorption efficiency for macromolecular organic pollutants has been significantly improved. That is because CFA enriches the pore structure of zeolite, which can accommodate large organic pollutant molecules. Therefore, according to the above analysis, the introduction of CFA can enhance the adsorption capacity of zeolite for macromolecular organic pollutants.

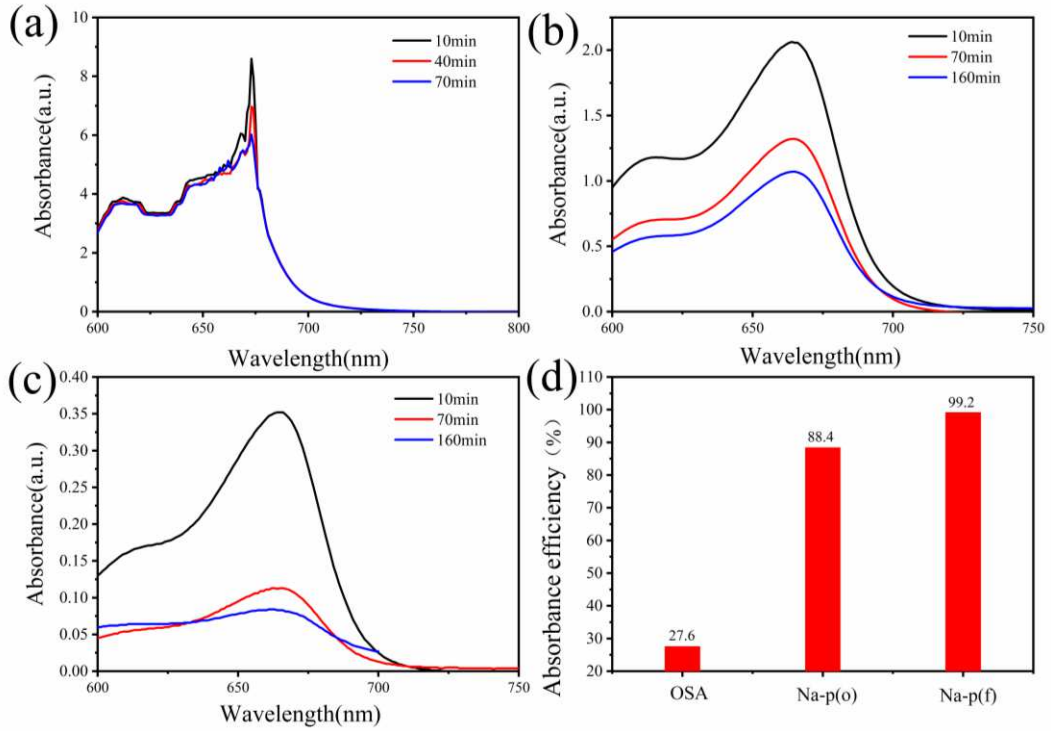


Fig. 6. The uw absorption of MB aqueous solution at different reaction times for (a) OSA; (b) Na-p(o); **(c)** Na-p(f); **(d) The adsorption efficiency of three samples.**

3.2.2. adsorption mode

The effect of zeolite on the adsorption process of MB by adsorbent is analyzed by fitting Langmuir and Freundlich adsorption isotherms. The Langmuir adsorption isotherm assumes that the surface properties of the adsorbent are uniform [37]. If one adsorbate occupies the position of the adsorbent, the other adsorbate cannot take the same adsorption position, thus achieving adsorption equilibrium [38]. The Langmuir isotherm can be obtained by the following equation. [39]:

$$1/Q_e = 1/Q_{\max} + 1/(K_l Q_{\max} C_e) \qquad (4)$$

Here "Q_e" represents the amount of adsorbent adsorbed at equilibrium (mg/g of adsorbate), "Q_{max}" is the maximum adsorbed amount of mono-layer that has completely adsorbed on the adsorbent (mg/g), "K_L" corresponds to the Langmuir isotherm constant (L/mg), and "C_e" is the concentration of the adsorption solution at equilibrium (mg/L). The values of "K_L" and "Q_{max}" (summarized in Table 1) can be derived from linear plots of "C_e/Q_e"

against "C_e", with the slopes and intercepts calculated.

Table 1 Parameters associated with Langmuir and Freundlich adsorption isotherm models

Samples	Langmuir			Freundlich		
	R^2	Q_{max} (mg/g)	K_l (L/mg)	R^2	*1/n*	K_f
OSA	0.91	16.6	0.07	0.83	0.56	1.76
Na-p(o)	0.98	33.3	1	0.67	0.21	17.8
Na-p(f)	0.97	55.5	10.6	0.94	0.32	48.4

At suitable concentrations, the C_e/Q_e points show a linear increase with the C_e value points by fitting the adsorption data of MB. The R^2 values for OSA, Na-p(o), and Na-p(f) are 0.91, 0.97, and 0.98, respectively, indicating that the Langmuir model is appropriate for adsorption of MB.

The Freundlich isotherm is an empirical equation assuming that the adsorption process corresponds to multi-layer adsorption [40], where adsorbate molecules are adsorbed on non-uniform surfaces due to the lack of sufficient adsorption sites [41]. The linear equation for the Freundlich adsorption isotherm can be obtained by the following relationship. [42]:

$$\log Q_e = \log K_f + (1/n)\log C_e \qquad (5)$$

The Freundlich isotherm constant (mg/g) is identified as "K_f" with "*1/n*" denoting the intensity of adsorption, categorized as either irreversible (1/n = 0), favorable (0 < 1/n < 1) or unfavorable (1/n > 1) [43]. These values can be calculated via a linear plot of "$logQ_e$" against "$logC_e$", which are summarized in Table .1. The intercepts and slopes of the linear plot of "$logQ_e$" and "$logC_e$" can then be determined. After calculating, all values of "*1/n*" fall within the range of 0 to 1, they are indicating a favorable process of adsorption.

The fitting curves of Langumires and Freundlich adsorption isotherm are shown in Fig. 7 (a) and (b). It is worth noting that the linear coefficient R^2 of the Freundlich model is lower than the Langmuir model. This suggests that the Freundlich isotherm model is unsuitable for MB adsorption and that the process aligns better with mono-layer adsorption.

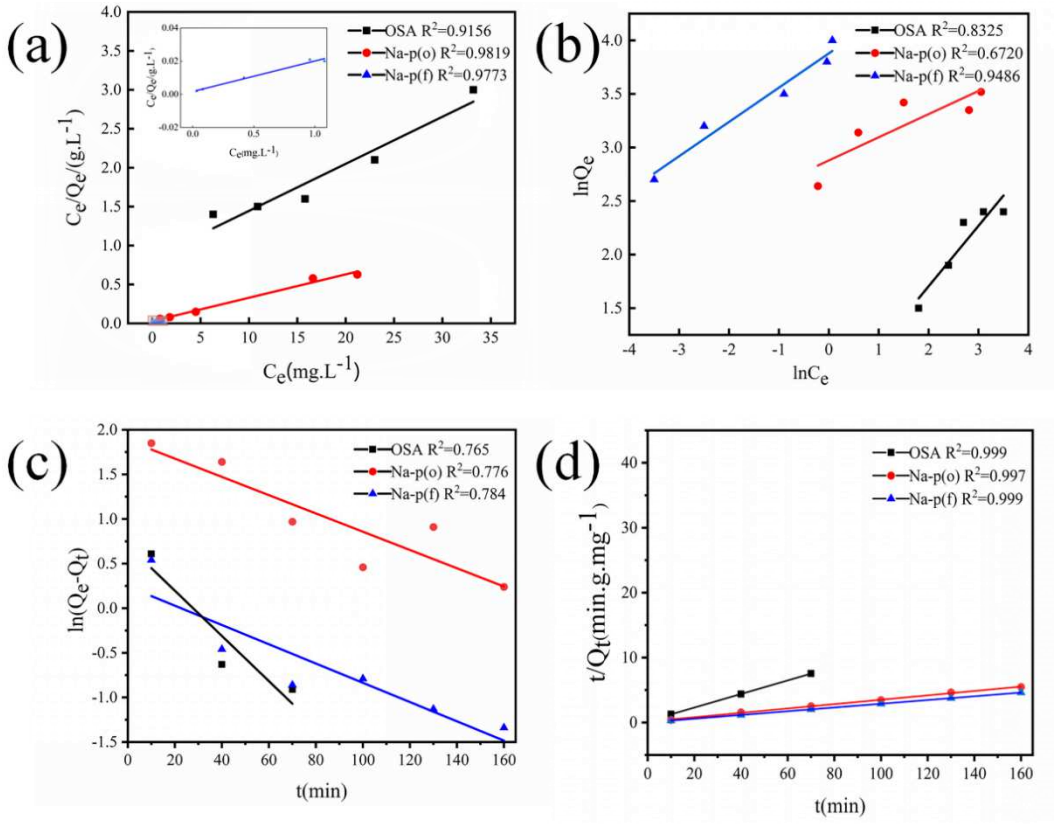


Fig. 7. (a) The fitting curve of langumires adsorption isotherm; (b) The fitting curve of Freundlich adsorption isotherm; (c) The pseudo-first-order kinetic fitting curve of ;(d) The pseudo-second-order kinetic of three samples

The adsorption rate is the main factor to describe the efficiency of zeolite adsorption, which is obtained by calculating the absorption amount of zeolite per unit weight and time in an aqueous solution. [44, 45]. There exist two widely used kinetic models that assist in predicting the adsorption mechanism and determining the adsorption rate. Pseudo-first-order and pseudo-second-order interparticle diffusion models are utilized to accurately fit the experimental data [46]. The pseudo-first-order equation assumes that the experimental data relates only to the initial phase of the adsorption process. However, this approach is not able to account for the entire time scale of the adsorption behavior [47]. In contrast, the pseudo-second-order model assesses the adsorption behavior's suitability throughout the entire period. The pseudo-first-order equation is presented as the following equation [48]:

$$\log(Q_e - Q_t) = \log Q_e - (k_1 t)/2.303 \qquad (6)$$

Where Q_e (mg/g) and Q_t (mg/g) represent the adsorbed amounts on the adsorbent at equilibrium and time t, respectively. Equilibrium rate constant K_1 can be determined from the slope and intercept of the linear plot of $log(Q_e - Q_t)$ versus t, where the values of Q_e and K_1 are summarized in Table .2. The pseudo-second-order dynamic model obeys the following equation [49]:

$$(t/Q_t) = [1/(k_2 Q_e^{\ 2})] + t/Q_e \qquad (7)$$

Here, "k_2" (g/mg/min) represents the equilibrium rate constant for the pseudo-second-order rea. Similarly, the "Q_e" and "k_2" values (Table .2) can be determined through linear plots of "t/Q_t" versus slopes and intercepts. The pseudo-first and second-order fitting curves of three samples are illustrated in Fig(c) and (d). The linear correlation coefficients (R^2) for all pseudo-second-order are significantly higher than those of pseudo-first-order (0.76-0.78), indicating that pseudo-second-order is the best kinetic model. Furthermore, the Q_e values calculated using the pseudo-second-order model are more closer to the experimental data, providing further evidence that the pseudo-second-order model is the most suitable.

Table 2 Parameters associated with the pseudo-first-order dynamics and pseudo-second-order dynamics models

Samples	Pseudo-1st-order kinetic model			Pseudo-2nd-order kinetic model		
	R^2	Q_e (mg/g)	K_1 (min)$^{-1}$	R^2	Q_e (mg/g)	K_2 (g/mg/min)
OSA	0.76	2.07	0.057	0.999	9.5	0.049
Na-p(o)	0.77	6.5	0.023	0.997	29.6	0.008
Na-p(f)	0.78	1.27	0.024	0.999	34.6	0.074

4. Conclusions

In summary, Na-p zeolites were successfully prepared from OSA and CFA as raw materials. The results show that the MB adsorption efficiency of zeolite prepared from OSA and CFA is improved compared with the zeolite synthesized from pure OSA. After adding CFA to the OSA, the crystallinity of the Na-p(f) zeolite is 86.32%, the specific surface area is 59.6 m^2/g, the adsorption efficiency for MB is 99.2%. The thermodynamic and kinetic results of adsorption indicate that the adsorption process of MB by OSA and Na-p(f) zeolite belongs to single-layer spontaneous physical adsorption, and the pseudo-second-order model is the best kinetic mode. The increase of adsorption efficiency of Na-p(f) zeolite is related to the enrichment of pore structure after the addition of CFA to OSA. These results obtained in the present study prove that zeolite can be regarded as a candidate for the treatment of waste water and organic dyes.

Acknowledgment

This work funded by Department of Science and Technology of JiLin Province (20220508042RC, 20220203109SF,YDZJ202301ZYTS547 and 20230203170SF) ; Jilin Province Development and Reform Commission (2022C040-5, 2023C033-4) And Education Department of Jilin Province (JJKH20210300KJ, JJKH20220267CY)

References

[1] S. Yan, H. Zhang, Z. Yang, M. Tang, M. Zhang, C. Du, H.-L. Cui, D. Wei, Transformation and dehydration kinetics of methylene blue hydrates detected by terahertz time-domain spectroscopy, RSC Adv., 7 (2017) 41667-41674. http://dx.doi.org/10.1039/c7ra07118c

[2] S.W. Lee, H.C. Han, Methylene Blue Application to Lessen Pain: Its Analgesic Effect and Mechanism, Frontiers in Neuroscience, 15 (2021). http://dx.doi.org/10.3389/fnins.2021.663650
[3] L.M. Pereira, G.B.e. Portapilla, G.T.P. Brancini, B. Possato, C.s.M. Bronzon da Costa, P.r.G. Abreu-Filho, M. Wainwright, A.P.c. Yatsuda, G.Ã.L. Braga, The potential of phenothiazinium dyes as cytotoxicity markers in cisplatin-treated cells, Scientific Reports, 13 (2023) 10203.
[4] A. Ebrahimian Pirbazari, E. Saberikhah, S.S. Habibzadeh Kozani, Fe3O4–wheat straw: preparation, characterization and its application for methylene blue adsorption, Water Resour. Ind., 7-8 (2014) 23-37. http://dx.doi.org/10.1016/j.wri.2014.09.001
[5] T.S. Alomar, N. AlMasoud, G. Sharma, Z.A. ALOthman, M. Naushad, Incorporation of trimetallic nanoparticles to the SiO2 matrix for the removal of methylene blue dye from aqueous medium, Journal of Molecular Liquids, 336 (2021) 116274.
[6] T. Liu, Y. Li, Q. Du, J. Sun, Y. Jiao, G. Yang, Z. Wang, Y. Xia, W. Zhang, K. Wang, H. Zhu, D. Wu, Adsorption of methylene blue from aqueous solution by graphene, Colloids Surf., B, 90 (2012) 197-203. http://dx.doi.org/10.1016/j.colsurfb.2011.10.019
[7] M. Rafatullah, O. Sulaiman, R. Hashim, A. Ahmad, Adsorption of methylene blue on low-cost adsorbents: A review, J. Hazard. Mater., 177 (2010) 70-80. http://dx.doi.org/10.1016/j.jhazmat.2009.12.047
[8] L. Meili, P.V.S. Lins, M.T. Costa, R.L. Almeida, A.K.S. Abud, J.I. Soletti, G.L. Dotto, E.H. Tanabe, L. Sellaoui, S.H.V. Carvalho, A. Erto, Adsorption of methylene blue on agroindustrial wastes: Experimental investigation and phenomenological modelling, Prog. Biophys. Mol. Biol., 141 (2019) 60-71. http://dx.doi.org/10.1016/j.pbiomolbio.2018.07.011
[9] S. Wang, Z.H. Zhu, A. Coomes, F. Haghseresht, G.Q. Lu, The physical and surface chemical characteristics of activated carbons and the adsorption of methylene blue from wastewater, J. Colloid Interface Sci., 284 (2005) 440-446. http://dx.doi.org/10.1016/j.jcis.2004.10.050
[10] G. Crini, E. Lichtfouse, Advantages and disadvantages of techniques used for wastewater treatment, Environmental Chemistry Letters, 17 (2018) 145-155. http://dx.doi.org/10.1007/s10311-018-0785-9
[11] J.M. Dias, M.C.M. Alvim-Ferraz, M.F. Almeida, J. Rivera-Utrilla, M. Sánchez-Polo, Waste materials for activated carbon preparation and its use in aqueous-phase treatment: A review, J. Environ. Manage., 85 (2007) 833-846. http://dx.doi.org/10.1016/j.jenvman.2007.07.031
[12] W. Salah Alaloul, M. Al Salaheen, A.B. Malkawi, K. Alzubi, A.M. Al-Sabaeei, M. Ali Musarat, Utilizing of oil shale ash as a construction material: A systematic review, Constr. Build. Mater., 299 (2021). http://dx.doi.org/10.1016/j.conbuildmat.2021.123844
[13] Q. Lü, X. Dong, Z. Zhu, Y. Dong, Environment-oriented low-cost porous mullite ceramic membrane supports fabricated from coal gangue and bauxite, J. Hazard. Mater., 273 (2014) 136-145. http://dx.doi.org/10.1016/j.jhazmat.2014.03.026
[14] J.D.N. Pone, K.A.A. Hein, G.B. Stracher, H.J. Annegarn, R.B. Finkleman, D.R. Blake, J.K. McCormack, P. Schroeder, The spontaneous combustion of coal and its by-products in the Witbank and Sasolburg coalfields of South Africa, Int. J. Coal Geol., 72 (2007) 124-140. http://dx.doi.org/10.1016/j.coal.2007.01.001
[15] S. Liu, X. Chen, W. Ai, C. Wei, A new method to prepare mesoporous silica from coal gasification fine slag and its application in methylene blue adsorption, J. Cleaner Prod., 212 (2019) 1062-1071. http://dx.doi.org/10.1016/j.jclepro.2018.12.060

[16] S.-x. Bai, L.-m. Zhou, Z.-b. Chang, C. Zhang, M. Chu, Synthesis of Na-X zeolite from Longkou oil shale ash by alkaline fusion hydrothermal method, Carbon Resour. Convers., 1 (2018) 245-250. http://dx.doi.org/10.1016/j.crcon.2018.08.005
[17] R. Shawabkeh, A. Al-Harahsheh, M. Hami, A. Khlaifat, Conversion of oil shale ash into zeolite for cadmium and lead removal from wastewater, Fuel, 83 (2004) 981-985. http://dx.doi.org/10.1016/j.fuel.2003.10.009
[18] H. Li, F. Zheng, J. Wang, J. Zhou, X. Huang, L. Chen, P. Hu, J.-m. Gao, Q. Zhen, S. Bashir, J.L. Liu, Facile preparation of zeolite-activated carbon composite from coal gangue with enhanced adsorption performance, Chem. Eng. J., 390 (2020). http://dx.doi.org/10.1016/j.cej.2020.124513
[19] W. Bao, L. Liu, H. Zou, S. Gan, X. Xu, G. Ji, G. Gao, K. Zheng, Removal of Cu2+ from Aqueous Solutions Using Na-A Zeolite from Oil Shale Ash, Chin. J. Chem. Eng., 21 (2013) 974-982. http://dx.doi.org/10.1016/s1004-9541(13)60529-7
[20] T.T. Wałek, F. Saito, Q. Zhang, The effect of low solid/liquid ratio on hydrothermal synthesis of zeolites from fly ash, Fuel, 87 (2008) 3194-3199. http://dx.doi.org/10.1016/j.fuel.2008.06.006
[21] T.V. Ojumu, P.W. Du Plessis, L.F. Petrik, Synthesis of zeolite A from coal fly ash using ultrasonic treatment – A replacement for fusion step, Ultrason. Sonochem., 31 (2016) 342-349. http://dx.doi.org/10.1016/j.ultsonch.2016.01.016
[22] M. Jafarnejad, M.D. Asli, F.A. Taromi, M. Manoochehri, Synthesis of multi-functionalized Fe3O4-NH2-SH nanofiber based on chitosan for single and simultaneous adsorption of Pb(II) and Ni(II) from aqueous system, Int. J. Biol. Macromol., 148 (2020) 201-217. http://dx.doi.org/10.1016/j.ijbiomac.2020.01.017
[23] S.G. Muntean, M.A. Nistor, R. Ianoș, C. Păcurariu, A. Căpraru, V.-A. Surdu, Combustion synthesis of Fe3O4/Ag/C nanocomposite and application for dyes removal from multicomponent systems, Appl. Surf. Sci., 481 (2019) 825-837. http://dx.doi.org/10.1016/j.apsusc.2019.03.161
[24] Y. Liu, C. Yan, J. Zhao, Z. Zhang, H. Wang, S. Zhou, L. Wu, Synthesis of zeolite P1 from fly ash under solvent-free conditions for ammonium removal from water, J. Cleaner Prod., 202 (2018) 11-22. http://dx.doi.org/10.1016/j.jclepro.2018.08.128
[25] H. Wang, K. Feng, Q. Sun, Effect of calcium carbonate on the preparation of glass ceramic foams from water-quenched titanium-bearing blast furnace slag and waste glass, Adv. Appl. Ceram., 117 (2018) 312-318. http://dx.doi.org/10.1080/17436753.2017.1412120
[26] J. Qu, J. Zhang, H. Li, S. Li, A high value utilization process for coal gasification slag: Preparation of high modulus sodium silicate by mechano-chemical synergistic activation, Sci. Total Environ., 801 (2021). http://dx.doi.org/10.1016/j.scitotenv.2021.149761
[27] S.O. Otieno, F.O. Kengara, C.O. Kowenje, R. Mokaya, Hydrothermal synthesis of zeolites using silica extracted from tropical volcanic ash, Mater Adv., 4 (2023) 2292-2300. http://dx.doi.org/10.1039/d3ma00065f
[28] D. Vaičiukynienė, L. Jakevičius, A. Kantautas, V. Vaitkevičius, V. Vaičiukynas, K. Dvořák, Conversion of silica by-product into zeolites by thermo-sonochemical treatment, Ultrason. Sonochem., 72 (2021). http://dx.doi.org/10.1016/j.ultsonch.2020.105426
[29] P. Larkin, Infrared and Raman spectroscopy: principles and spectral interpretation, Elsevier2017.
[30] E. Smidt, K. Meissl, The applicability of Fourier transform infrared (FT-IR) spectroscopy in waste management, Waste management, 27 (2007) 268-276.

[31] C. Wang, J. Yu, K. Feng, H. Guo, L. Wang, Alkali treatment to transform natural clinoptilolite into zeolite Na–P: Influence of NaOH concentration, J. Phys. Chem. Solids, 168 (2022). http://dx.doi.org/10.1016/j.jpcs.2022.110827
[32] M. Alkan, Ç. Hopa, Z. Yilmaz, H. Güler, The effect of alkali concentration and solid/liquid ratio on the hydrothermal synthesis of zeolite NaA from natural kaolinite, Appl. Surf. Sci., 86 (2005) 176-184. http://dx.doi.org/10.1016/j.micromeso.2005.07.008
[33] T. Revathi, R. Jeyalakshmi, Fly ash–GGBS geopolymer in boron environment: A study on rheology and microstructure by ATR FT-IR and MAS NMR, Constr. Build. Mater., 267 (2021). http://dx.doi.org/10.1016/j.conbuildmat.2020.120965
[34] Z. Huo, X. Xu, Z. Lü, J. Song, M. He, Z. Li, Q. Wang, L. Yan, Synthesis of zeolite NaP with controllable morphologies, Microporous Mesoporous Mater., 158 (2012) 137-140. http://dx.doi.org/10.1016/j.micromeso.2012.03.026
[35] C. Sanchez, C. Boissiere, D. Grosso, C. Laberty, L. Nicole, Design, synthesis, and properties of inorganic and hybrid thin films having periodically organized nanoporosity, Chem. Mater., 20 (2008) 682-737.
[36] A.A. Marhoon, S.A. Hasbullah, N. Asikin-Mijan, W.N.A.W. Mokhtar, Hydrothermal synthesis of high-purity zeolite X from coal fly ash for heavy metal removal: Kinetic and isotherm analysis, Adv. Powder Technol., 34 (2023). http://dx.doi.org/10.1016/j.apt.2023.104242
[37] M.A. Al-Ghouti, D.A. Da'ana, Guidelines for the use and interpretation of adsorption isotherm models: A review, J. Hazard. Mater., 393 (2020). http://dx.doi.org/10.1016/j.jhazmat.2020.122383
[38] G.K. Rajahmundry, C. Garlapati, P.S. Kumar, R.S. Alwi, D.-V.N. Vo, Statistical analysis of adsorption isotherm models and its appropriate selection, Chemosphere, 276 (2021). http://dx.doi.org/10.1016/j.chemosphere.2021.130176
[39] E. Alver, A.Ü. Metin, Anionic dye removal from aqueous solutions using modified zeolite: Adsorption kinetics and isotherm studies, Chem. Eng. J., 200-202 (2012) 59-67. http://dx.doi.org/10.1016/j.cej.2012.06.038
[40] S. Chen, W. Shen, F. Yu, H. Wang, Kinetic and thermodynamic studies of adsorption of Cu2+ and Pb2+ onto amidoximated bacterial cellulose, Polym. Bull., 63 (2009) 283-297. http://dx.doi.org/10.1007/s00289-009-0088-1
[41] M. Auta, B.H. Hameed, Modified mesoporous clay adsorbent for adsorption isotherm and kinetics of methylene blue, Chem. Eng. J., 198-199 (2012) 219-227. http://dx.doi.org/10.1016/j.cej.2012.05.075
[42] X. Lu, D. Shi, J. Chen, Sorption of Cu2+ and Co2+ using zeolite synthesized from coal gangue: isotherm and kinetic studies, Environ. Earth Sci., 76 (2017). http://dx.doi.org/10.1007/s12665-017-6923-z
[43] F. Togue Kamga, Modeling adsorption mechanism of paraquat onto Ayous (Triplochiton scleroxylon) wood sawdust, Appl. Water Sci, 9 (2018). http://dx.doi.org/10.1007/s13201-018-0879-3
[44] L. Roshanfekr Rad, M. Anbia, Zeolite-based composites for the adsorption of toxic matters from water: A review, J. Environ. Chem. Eng., 9 (2021). http://dx.doi.org/10.1016/j.jece.2021.106088
[45] C. Feng, E. Jiaqiang, W. Han, Y. Deng, B. Zhang, X. Zhao, D. Han, Key technology and application analysis of zeolite adsorption for energy storage and heat-mass transfer process: A review, Renewable Sustainable Energy Rev., 144 (2021) 110954.
[46] S. Loganathan, M. Tikmani, S. Edubilli, A. Mishra, A.K. Ghoshal, CO2 adsorption kinetics on mesoporous silica under wide range of pressure and temperature, Chem. Eng. J., 256 (2014) 1-8. http://dx.doi.org/10.1016/j.cej.2014.06.091

[47] W. Rudzinski, W. Plazinski, Kinetics of solute adsorption at solid/solution interfaces: a theoretical development of the empirical pseudo-first and pseudo-second order kinetic rate equations, based on applying the statistical rate theory of interfacial transport, The Journal of Physical Chemistry B, 110 (2006) 16514-16525.
[48] J.-P. Simonin, On the comparison of pseudo-first order and pseudo-second order rate laws in the modeling of adsorption kinetics, Chem. Eng. J., 300 (2016) 254-263.
http://dx.doi.org/10.1016/j.cej.2016.04.079
[49] T.H. Tran, A.H. Le, T.H. Pham, D.T. Nguyen, S.W. Chang, W.J. Chung, D.D. Nguyen, Adsorption isotherms and kinetic modeling of methylene blue dye onto a carbonaceous hydrochar adsorbent derived from coffee husk waste, Sci. Total Environ., 725 (2020).
http://dx.doi.org/10.1016/j.scitotenv.2020.138325